







## Magnetic nanodoping: Atomic control of spin states in cobalt doped silver clusters

Vicente Zamudio-Bayer <sup>1</sup>, Konstantin Hirsch,<sup>1</sup> Lei Ma,<sup>2</sup> Kobe De Knijf <sup>3</sup>, Xiaoshan Xu,<sup>4,5</sup> Arkadiusz Ławicki,<sup>1</sup> Akira Terasaki <sup>6</sup>, Piero Ferrari <sup>3</sup>, Bernd von Issendorff,<sup>7</sup> Peter Lievens <sup>3,\*</sup>, Walt A. de Heer,<sup>8</sup> J. Tobias Lau,<sup>1,7,†</sup> and Ewald Janssens <sup>3</sup>

<sup>1</sup>*Abteilung für Hochempfindliche Röntgenspektroskopie, Helmholtz-Zentrum Berlin für Materialien und Energie, Albert-Einstein-Straße 15, 12489 Berlin, Germany*

<sup>2</sup>*Tianjin International Center for Nanoparticles and Nanosystems, Tianjin University, 92 Weijin Road, Nankai District, Tianjin 300072, China*

<sup>3</sup>*Quantum Solid-State Physics, KU Leuven, Celestijnenlaan 200d, 3001 Leuven, Belgium*


<sup>4</sup>*Department of Physics and Astronomy, University of Nebraska-Lincoln, Lincoln, Nebraska 68588-0299, USA*

<sup>5</sup>*Nebraska Center for Materials and Nanoscience, University of Nebraska-Lincoln, Lincoln, Nebraska 68588-0299, USA*

<sup>6</sup>*Department of Chemistry, Faculty of Science, Kyushu University, 744 Motoooka, Nishi-ku, Fukuoka 819-0395, Japan*

<sup>7</sup>*Physikalisches Institut, Universität Freiburg, Hermann-Herder-Straße 3a, 79104 Freiburg, Germany*

<sup>8</sup>*School of Physics, Georgia Institute of Technology, Atlanta, Georgia 30332, USA*

 (Received 6 September 2022; revised 6 May 2023; accepted 20 June 2023; published 15 August 2023)

The interaction of magnetic dopants with delocalized electron states can result in interesting many-body physics. Here, the magnetic properties of neutral and charged finite silver metal host clusters with a magnetic cobalt atom impurity were investigated experimentally by exploiting the complementary methods of Stern-Gerlach molecular beam deflection and x-ray magnetic circular dichroism spectroscopy and are accompanied by density functional theory calculations and charge transfer multiplet simulations. The influence of the number of valence electrons and the consequences of impurity encapsulation were addressed in free size-selected, singly cobalt-doped silver clusters  $\text{CoAg}_n^{0,+}$  ( $n = 2-15$ ). Encapsulation of the dopant facilitates the formation of delocalized electronic shells with complete hybridization of the impurity  $3d$ - and the host  $5s$ -derived orbitals, which results in impurity valence electron delocalization, effective spin relaxation, and a low-spin ground state. In the exohedral size regime, spin pairing in the free electron gas formed by the silver  $5s$  electrons is the dominating driving force determining the local  $3d$  occupation of the impurity and therefore, adjusting the spin magnetic moment accordingly.

DOI: [10.1103/PhysRevResearch.5.033103](https://doi.org/10.1103/PhysRevResearch.5.033103)

### I. INTRODUCTION

The interaction of localized spins with delocalized electrons is of interest from a fundamental point of view but also for its technological relevance [1–3]. Depending on the strength of this interaction, the quenching of magnetic moments, the existence of spin-glasses, or the Kondo effect [4] can occur. The latter has been generalized in the Anderson model to the interaction of a localized state with a continuum of delocalized bands as an interplay of on-site Coulomb interaction and hybridization [5]. This type of interaction is not limited to bulk systems but also plays a role for individual atoms adsorbed on metal surfaces and in quantum dot systems [6,7].

We aim for atomic-level control of hybridization, as offered by free, size-selected clusters of coinage metals approximat-

ing quasifree electrons that interact with a magnetic impurity. Previous studies that experimentally probed the magnetic properties of free magnetically doped clusters have been limited to the small size regime where the transition metal atom is exohedral, [8,9] or to host materials that are not well described as simple metals such as silicon [10], niobium [11], or tin [12]. In contrast to the latter, silver as a host metal approximates a free electron gas because the energy of its  $4d$  orbitals is considerably lower than the  $3d$  orbitals in copper, or  $5d$  orbitals in gold, resulting in valence orbitals of almost pure  $5s$  character [13]. However, results on the spin multiplicity of  $3d$  transition metal-doped silver clusters have mostly been obtained indirectly by photofragmentation mass spectrometry, reactivity studies, photoelectron spectroscopy, or computational studies [14–23]. Although these studies focused on structural properties, it has been suggested that  $\text{CoAg}_{10}^+$  is diamagnetic with closed electronic shells and adopts an endohedral structure [14,18]. Furthermore, density functional theory (DFT) studies found a high-spin state (triplet or quartet) as the ground state for neutral  $\text{CoAg}_n$  with  $n = 2-5$ , 7 and a low-spin as the ground state for  $n = 6, 8, 9$  (doublet and singlet) [22,24]. Additional insights on the electronic and magnetic structure of transition metal doped silver clusters has been obtained from the investigation of small  $\text{VAg}_n^{0,+}$  clusters using DFT [16]. It was reported that while  $\text{VAg}_n^{0,+}$

\*peter.lievens@kuleuven.be

†tobias.lau@helmholtz-berlin.de

Published by the American Physical Society under the terms of the [Creative Commons Attribution 4.0 International license](https://creativecommons.org/licenses/by/4.0/). Further distribution of this work must maintain attribution to the author(s) and the published article's title, journal citation, and DOI.

clusters with  $n \leq 11$  have high-spin ground states, clusters with  $n \geq 13$  exhibit singlet and doublet states for even and odd numbers of valence electrons in the clusters, respectively [16]. A gradual decrease of the spin multiplicity in a size regime of intermediate  $5s - 3d$  hybridization is predicted to set in at  $n = 8$ , presumably triggered by increasing coordination as the dopant becomes gradually encapsulated with increasing cluster size. For  $n \geq 13$  strong hybridization of dopant and host states sets in and the electronic structure can be well described by the Clemenger-Nilsson model [25] when considering all valence electrons of dopant and host atoms. So far, however, there is no experimental confirmation of the effect of the size-dependent increase of the  $s-d$  hybridization on the magnetic properties of doped silver clusters.

We employ Stern-Gerlach deflection of neutral molecular beams (Refs. [12,26] and references therein) of  $\text{CoAg}_n$  clusters and x-ray magnetic circular dichroism (XMCD) spectroscopy of  $\text{CoAg}_n^+$  clusters in an ion trap [27–30], which are complementary techniques that provide direct access to the magnetic and electronic properties of size-selected clusters in their respective charge state. Stern-Gerlach deflection can deliver information on the spin relaxation behavior and on the total magnetic moment of neutral clusters [12,31–34], while x-ray absorption spectroscopy (XAS) probes the dopant’s local electronic structure, and XMCD provides element and orbital specific contributions to the magnetic moment [8,10,27].

Here, we report on the spin magnetic moment for neutral and cationic clusters for sizes  $n = 2-15$  covering the whole region of exohedral to endohedral doping. For pure and cobalt-doped silver clusters that exhibit a doublet state we find that cobalt doping enhances the spin relaxation. Additionally, in the endohedral size regime ( $n = 10-15$ ) [18], the dopant’s electronic structure in  $\text{CoAg}_n$  is almost size independent due to the delocalization of the Co  $3d$  and  $4s$  electrons accompanied with low spin configurations, which is very distinct from silicon [10], niobium [11], or tin [12] doped clusters where the dopant’s local electronic structure strongly changes with cluster size. In the particular case of  $\text{CoAg}_9^+$  valence electron delocalization is achieved without involvement of the dopant’s  $3d$  electrons, which remain localized as evidenced by the integer  $3d$  occupation. We elucidate that the size-dependent  $3d-5s$  hybridization results from an intricate interplay of the occupation of the cluster’s electronic shells, the geometric structure of the cluster, and the position of the cobalt dopant atom (exo- or endohedral) within the cluster. This ultimately determines the magnetic properties of  $\text{CoAg}_n$  clusters.

## II. EXPERIMENTAL METHODS

### A. Cluster production

Cobalt doped silver clusters, either neutral or cationic, were produced by laser vaporization or magnetron sputtering. In the laser vaporization source, the metal was brought into the gas phase through laser ablation of an alloy target. The alloy target was prepared in a UHV radio-frequency induction furnace from a mixture of isotopically enriched silver,  $^{107}\text{Ag}$ , and cobalt powder in a  $m_{\text{Ag}} : m_{\text{Co}} = 100 : 1.5$  mass ratio. In the magnetron sputtering source, a cobalt target (99.9% purity) covered by a perforated silver target (99.9% purity) as mask,

was sputtered with argon ions. The size of the holes in the silver sputtering target and the Ag:Co ratio in the alloy target were optimized to minimize multiple cobalt doping of the silver clusters. Both cluster sources operate at low temperature. The laser vaporization source was maintained at  $T = 20$  K by a temperature controlled closed cycle cryogenic refrigerator. For the magnetron sputtering source, a liquid-nitrogen-filled cooling jacket guaranteed a stable source temperature. The cooling in both sources reduces any possible contamination and allows for better control of the cluster size distribution.

### B. Stern-Gerlach deflection

In the molecular beam setup for Stern-Gerlach neutral cluster deflection [35,36] a helium-carried cluster beam is skimmed and collimated to a width of about 0.3 mm before entering an inhomogeneous magnetic field produced by the Stern-Gerlach magnet (magnetic field  $B = 0.47$  T and magnetic field gradient  $dB/dz = 124$  T/m; magnet length 0.125 m). After deflection (distance between deflector and ionization of 0.80 m), the clusters are photoionized with an  $\text{F}_2$  excimer laser ( $\lambda = 157$  nm) and detected in a position-sensitive time-of-flight mass spectrometer, which allows to detect simultaneously the mass and deflection of the clusters in the beam [37]. This method requires that mass resolution is traded for position sensitivity. In the Stern-Gerlach experiments, clusters are zero-field cooled.

### C. Ion trap x-ray spectroscopy

The x-ray spectroscopy experiments were performed with the ion trap end station at the BESSY II synchrotron radiation storage ring [10,27,30,38]. The ion beam was transmitted through a radio-frequency hexapole ion guide into a quadrupole mass filter. After mass selection, the clusters were accumulated in a cryogenic linear Paul trap and thermalized to 10–20 K by collisions with helium buffer gas at  $p \approx 10^{-4}$  mbar. The tunable, monochromatic x-ray beam was coupled on-axis into the ion trap for resonant excitation at the cobalt  $L_3$  absorption edge. This produced predominantly  $\text{Ag}_2^+$  and  $\text{Ag}^+$  photofragments, which were detected by a reflectron time-of-flight mass spectrometer. The incident photon energy was scanned from 774 to 790 eV to record photoion yield spectra that usually are almost proportional to the x-ray absorption cross section. The photon energy bandwidth was 500 meV and the scan step width was 200 meV. Photon energies are calibrated with an error of 0.5 eV. The ion yield signal was integrated over 12 s per energy step. For XMCD spectroscopy, which requires the magnetization of the  $\text{CoAg}_n^+$  cluster ion cloud in the trap, a superconducting solenoid around the liquid-helium cooled ion trap generated a homogeneous magnetic field of  $B = 5$  T in the ion trap volume. Ion yield spectra were then recorded for parallel and antiparallel alignment of the photon helicity and the magnetic field. The XMCD spectra are thus obtained for field-cooled clusters in thermal equilibrium with cold helium buffer gas. The presented x-ray absorption spectra result from averaging of at least three single scans per cluster size and photon beam helicity.

### III. COMPUTATIONAL METHODS

The electronic structures of three selected clusters,  $\text{CoAg}_9^+$ ,  $\text{CoAg}_{10}^+$ , and  $\text{CoAg}_9$ , were calculated using density functional theory, by utilizing the ORCA 5.03 software package [39]. The PBE functional [40] was employed in conjunction with the Def2-TZVPP basis set [41], together with the Stuttgart Def2-ECP pseudopotentials for silver [42], which explicitly treats 19 valence electrons. In contrast, all electrons were considered for the cobalt dopant atom. Dispersion forces were taken into account through the D3BJ dispersion-correction [43,44]. SCF cycles and geometry optimization both employed “tight” convergence criteria. The spin configurations implied from the experimental results were used.

The geometry of the neutral  $\text{CoAg}_9$  cluster has been investigated in Refs. [22,24], which disagree about the lowest-energy isomer. The structure of Ref. [24] was found to be the lowest-energy isomer at our level of theory. Since the geometries of the cationic  $\text{CoAg}_9^+$  and  $\text{CoAg}_{10}^+$  clusters have not been studied before, we performed a structural search. Different initial geometries were constructed by randomly positioning the atoms in the cluster followed by optimization at the PBE/Def2-SVP level of theory. Afterwards, the lower-energy isomers were reoptimized at the PBE/Def2-TZVPP level. The putative lowest-energy isomers are those presented in the rest of the paper. A summary of the isomers identified with this procedure and their corresponding energetic ordering is presented in the Supplemental Material [46].

All symmetry adapted Hartree-Fock and charge transfer multiplet calculations were carried out with the CTM4XAS code [45] using the parameters given in the Supplemental Material [46]. Starting from the initial assumption of a single initial configuration of unperturbed (degenerate) cobalt  $3d$  orbitals, a moderate splitting of these orbitals was introduced by lowering the symmetry while monitoring the agreement between measured and simulated x-ray absorption and magnetic circular dichroism spectra. In cases of poor agreement, charge transfer was introduced to account for configuration interaction. The degree of a non-zero configuration interaction is reflected in the non-integer occupation of cobalt  $3d$  orbitals.

### IV. RESULTS

#### A. Stern-Gerlach deflection profiles of neutral cobalt-doped silver clusters

For neutral pure  $\text{Ag}_n$  clusters with  $n = 4 - 15$  the Stern-Gerlach response as a function of cluster size displays an odd-even alternation because the odd (even) numbered clusters have doublet (singlet) spin ground state, respectively (see Sec. I within the Supplemental Material [46]). The odd numbered silver clusters show a symmetrical splitting into two beamlets, with a deflection that decreases as the clusters become larger, in addition to a central undeflected fraction. The deflected fraction is attributed to vibrationally cold silver clusters (no relaxation through phonons) that have a total spin of  $1/2$  (no Orbach relaxation) [31]. The undeflected fraction is attributed to vibrationally excited clusters that undergo spin relaxation during the passage through the magnetic field.

The beam profiles of cobalt doped silver clusters  $\text{CoAg}_n$  with  $n = 4-15$ , with and without applied magnetic field, are

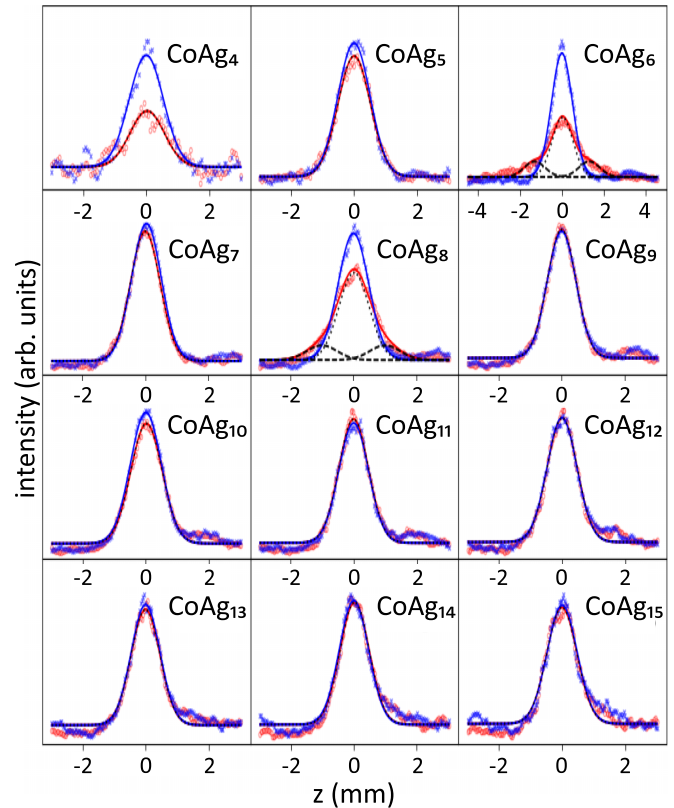


FIG. 1. Beam profiles of  $\text{CoAg}_n$  ( $n = 4-15$ ) clusters at  $T = 20$  K without magnetic field (blue crosses) and with applied magnetic field (red circles). The full lines are fits of the data without (blue line) and with (red line) magnetic field. The measured profiles were fitted by a single Gaussian. Only for the  $\text{CoAg}_6$  and  $\text{CoAg}_8$  profiles with applied magnetic field three Gaussians were used for the fit.

shown in Fig. 1. Only the beam profiles of the smallest clusters with an even number of silver atoms ( $n = 4, 6$ , and  $8$ ) show a clear response to the magnetic field. A small response may be present for  $n = 5, 7$ , and  $10$  as well. For  $\text{CoAg}_4$  only a strong decrease of undeflected intensity is observed, without additional beamlets appearing. For  $\text{CoAg}_6$  and  $\text{CoAg}_8$  the response is similar to the one described above for pure odd-numbered silver clusters: the undeflected intensity decreases and two additional, symmetrically deflected beamlets appear. We therefore, from the comparison with silver cluster deflection and based on earlier studies in literature [31], identify the spin state for  $\text{CoAg}_6$  and  $\text{CoAg}_8$  to be  $S = 1/2$ . An analogous fitting procedure as the one described for neutral silver clusters (see Sec. I within the Supplemental Material [46]) was used for the beam profiles of  $\text{CoAg}_6$  and  $\text{CoAg}_8$ , resulting in good agreement as shown in the figure. The comparison between even  $n$   $\text{CoAg}_n$  and odd  $n$   $\text{Ag}_n$  clusters shows that the deflected fraction is smaller in the former, although  $S = 1/2$  in both cases.

#### B. X-ray spectroscopy of cationic cobalt-doped silver clusters

An overview of the cobalt  $L_3$  x-ray absorption spectra of  $\text{CoAg}_n^+$  clusters with  $n = 2-12$  is shown in Fig. 2(a). The spectra result from  $2p_{3/2}-3d$  excitation into dipole-allowed, core-excited final states. The technique is therefore

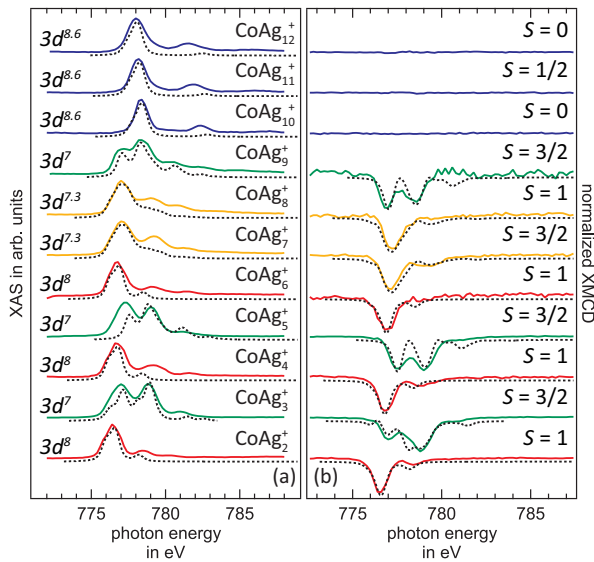


FIG. 2. X-ray absorption (a) and x-ray magnetic circular dichroism spectra (b) at the cobalt  $L_3$  edge of  $\text{CoAg}_n^+$  clusters ( $n = 2-12$ ). Additionally shown are Hartree-Fock and charge transfer multiplet calculations [dotted lines in (a) and (b)] alongside the extracted  $3d$  occupation (a). The spin states corresponding to the shown Hartree-Fock and charge transfer calculations occupation are also given (b).

sensitive to unoccupied valence states with considerable cobalt  $3d$  character, effectively probing the local electronic structure at the cobalt site. We additionally performed charge transfer multiplet calculations [45], which are also shown in Fig. 2(a) (parameters of the calculations can be found in Table S3 within the Supplemental Material [46]) in order to simulate the experimental spectra and to extract quantitative information on the occupation of  $3d$  derived orbitals. The x-ray absorption spectra in Fig. 2(a) show a clear cluster size dependence, with three distinct size ranges: small ( $n = 2-6$ ), intermediate ( $n = 7,8$ ), and large  $n \geq 10$  clusters.

For the small clusters ( $n = 2-6$ ), the spectral signature shows an odd-even pattern in the number  $n$  of silver atoms per cluster. The spectra of even-numbered  $\text{CoAg}_{2,4,6}^+$  can be well described by a Hartree-Fock calculation of an atomic-like  $3d^8$  cobalt configuration. The XAS of odd-numbered  $\text{CoAg}_{3,5}^+$  on the other hand can be reasonably well reproduced by a symmetry adapted but still integer  $3d^7$  atomic configuration of the dopant atom. All other valence electrons are of  $s$  character since the cobalt  $4s$  and silver  $5s$  readily hybridize.

As the cluster size increases to  $\text{CoAg}_7^+$  and  $\text{CoAg}_8^+$ , the odd-even pattern is less prominent and the XAS of these two clusters have similar shape. This is a result of an increased hybridization of the dopant and host states as indicated by the noninteger occupation of  $3d$  derived states, evident from simulation of experimental XAS of  $\text{CoAg}_{7,8}^+$  using a symmetry adapted charge transfer model. It should be noted that this is the same size range, which in the literature has been predicted to mark the transition from two to three dimensional like structures in neutral, doped silver clusters with varying transition metal impurity [16,22,24,47].

$\text{CoAg}_9^+$  again follows the odd-even pattern in the cobalt  $3d$  configuration of the small species. The experimental spectrum

can be simulated by a symmetry adapted model alone not involving any charge transfer. The resulting electronic configuration of the cobalt dopant is identified as  $3d^7$ .

Starting with the x-ray absorption spectrum of  $\text{CoAg}_{10}^+$ , the spectral signature changes dramatically and the spectrum now consists exclusively of one main line and one strongly blue-shifted satellite band, which are approximately 3.5 eV apart and have an intensity ratio of 5:1. For  $\text{CoAg}_{11}^+$  and  $\text{CoAg}_{12}^+$  the spectral shape remains basically unchanged. Nevertheless, the spectrum of  $\text{CoAg}_{10}^+$  stands out because for  $\text{CoAg}_{11}^+$  and  $\text{CoAg}_{12}^+$  the linewidth increases and a red-shifting of the two absorption bands is observed. The XAS of these endohedrally doped species can be simulated involving a parameter set indicating rather strong hybridization of the dopant's and host's electronic states. Hence, the extracted occupation of the  $3d$  derived orbitals is noninteger ( $3d^{8.6}$ ) and the hopping terms used in the simulation are larger by a factor of four compared to  $\text{CoAg}_{7,8}^+$ .

The cluster size dependence of the XMCD spectral shape mirrors the described trends for the x-ray absorption spectroscopy for  $n \leq 9$ , as can be seen in Fig. 2(b). The main observation is that while the XMCD signal is clearly visible for all clusters  $\text{CoAg}_n^+$  with  $n \leq 9$ , there is no XMCD signal for  $\text{CoAg}_{10}^+$  and larger clusters. This is consistent with the splitting of the  $3d$  orbitals due to the presence of a crystal field, which is only of moderate strength for  $n \leq 9$  (cf. Table S3 within the Supplemental Material [46]) and therefore too weak to induce a high- to low-spin transition in  $\text{CoAg}_n^+$ ,  $n \leq 9$  [48,49]. Hence, for clusters with  $n \leq 9$  the spin state is the highest possible compatible with the  $3d$  occupation, i.e.,  $S = 1$  for even  $n$  and  $S = 3/2$  for odd  $n$ .

## V. DISCUSSION

### A. Geometry and electronic structure of cobalt-doped silver cluster

Computational studies of the geometry of small neutral cobalt doped silver clusters  $\text{CoAg}_n$  have been reported [22,24], but are not fully consistent with each other. So far, no experimental information is available to resolve the disagreements. While there are differences in the exact atomic arrangements, there is consensus that  $\text{CoAg}_n$  clusters with  $n \leq 5$  are planar [22,24]. Since pure silver clusters with  $n \leq 6$  are known to be planar as well [50,51], the structural predictions are compatible with the picture of cobalt mimicking silver by delocalizing only the valence  $4s$  electrons, while the  $3d$  electrons remain essentially localized. Additionally, the formation of electronic shells is predicted to play a role in small neutral planar cobalt doped silver clusters such as  $\text{CoAg}_5$  [52]. In the electronic shell model, quantum confinement leads to the grouping of electrons into shells and to so-called “magic” numbers of electrons for closed-shell configurations [53]. As the cluster size increases, the predictions on the geometry of the lowest lying isomer deviate from each other. Particularly, for  $\text{CoAg}_9$  both an impurity encapsulating isomer [24] and an isomer with an open structure and exohedral dopant [22] have been predicted as the ground-state geometry. Encapsulation could be expected if the neutral  $\text{CoAg}_9$  system is best characterized as an 18 electron system with all silver  $5s$  and

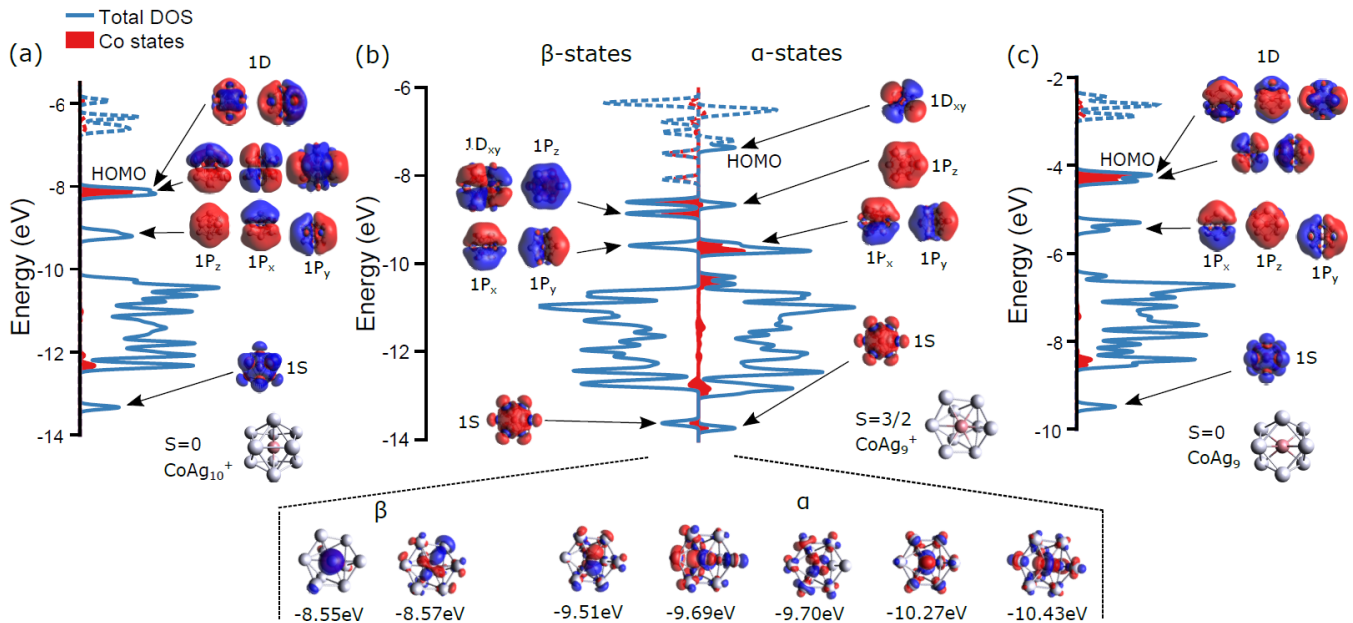


FIG. 3. Comparison of the density-of-states (DOS) of high-spin  $\text{CoAg}_9^+$  (b) and low-spin cationic  $\text{CoAg}_{10}^+$  (a) and neutral  $\text{CoAg}_9$  (c). The blue lines correspond to the total DOS (mainly contributed by silver 4d states), while the shaded red areas are projections of the total DOS onto the atomic orbitals of cobalt. The high-spin state of  $\text{CoAg}_9^+$  results from 10 delocalized valence electrons occupying electronic shells and seven localized 3d states (shown at the bottom of the figure). In the low-spin systems  $\text{CoAg}_{10}^+$  (a) and  $\text{CoAg}_9$  (c), the cobalt 3d states fully participate in the formation of electronic shells (18 delocalized valence electrons). For the isosurfaces a value of 0.01 a.u. was used.

cobalt 3d and 4s valence electrons delocalized, thus achieving electronic shell closure. Yet in Ref. [22], the encapsulation of cobalt by nine silver atoms resulted in elongated silver-silver bond lengths, reducing the binding energy.

For cationic cobalt doped silver clusters no systematic size dependent computational studies were performed. Several experimental studies, and complementary computational work for selected sizes, suggested that  $\text{CoAg}_{10}^+$  is the smallest cluster with an encapsulated cobalt atom [14,18,19]. In summary, whereas for the neutral  $\text{CoAg}_n$  clusters there is no agreement in the literature on the size of the smallest endohedrally doped cluster ( $n = 9$  vs  $n = 10$ ),  $\text{CoAg}_{10}^+$  is known to be the smallest cationic endohedrally cobalt doped silver cluster.

An approach for disentangling the number of valence electrons from the geometry is to investigate both neutral and cationic species. For this reason we performed DFT calculations for three selected clusters:  $\text{CoAg}_9^+$ ,  $\text{CoAg}_9$  and  $\text{CoAg}_{10}^+$ . The latter two systems have the same number of valence electrons if all silver 5s and cobalt 3d and 4s electrons are contributing to the cloud of delocalized electrons. In our calculations, for the neutral  $\text{CoAg}_9$  cluster, the isomer with an encapsulated cobalt impurity lies 0.45 eV lower in energy than the exohedral isomer. In contrast, for the cationic  $\text{CoAg}_9^+$  cluster, the open structure isomer is found 0.09 eV lower in energy. The lowest-energy isomers are depicted in Fig. 3.

### B. Spin states of cobalt-doped silver clusters

In neutral cobalt doped silver clusters, a clear response to the magnetic field is only observed for the smallest clusters with odd number of valence electrons ( $n = 4, 6$ , and 8). The

deflection pattern for  $\text{CoAg}_6$  and  $\text{CoAg}_8$  matches the blocked-spin behavior observed for odd numbered spin doublet silver clusters (see Sec. I within the Supplemental Material [46]), that is, those two clusters likely have  $S = 1/2$ , matching the computational predictions [24]. The strong response to the magnetic field in the beam profile of  $\text{CoAg}_4$  is likely explained by blocked spin  $S = 1/2$  behavior with the doublet beamlets being deflected out of the ionization region ( $6 \times 3 \text{ mm}^2$ ), but due to the low signal-to-noise ratio we cannot strictly discard weak quartet beamlets and the corresponding  $S = 3/2$  state.  $\text{CoAg}_4$  is predicted to have doublet and quartet states with the same energy within the accuracy of the computations [24]. For  $\text{CoAg}_5$  the deflected profile is slightly broader (FWHM = 1.28 mm) than the undeflected profile (1.14 mm). This may be an indication of a nonzero magnetic moment for this size, also in line with the computational predictions [22,24] of a triplet state with  $S = 1$ . The absence of a clear magnetic response for  $\text{CoAg}_7$  is consistent with either a singlet state, with no magnetic moment, or a triplet state that is subject to spin relaxation in the magnetic field since this would lead to a weak response below our experimental sensitivity under the current conditions. On the other hand, the experimental sensitivity allows to exclude higher spin states  $S \geq 2$  (see Supplemental Material [46] for maximal spin states that are compatible with the experimental sensitivity). Hence, for  $\text{CoAg}_7$ , we cannot determine whether  $S = 0$  or  $S = 1$  is present.

For all larger ( $n \geq 9$ ) cluster sizes no significant deflection was measured. This is consistent with the computational prediction that high spin states ( $S \geq 1$ ) are much higher in energy [24]. However, the lowest spin state for all even  $n$   $\text{CoAg}_n$  clusters is  $S = 1/2$  and would be expected to cause, as for

pure odd  $n$  pure  $\text{Ag}_n$  cluster, two symmetrical beamlets. The likely explanation for the absence of these beamlets is that the fraction of vibrationally cold clusters is small in those larger spin doublet clusters, causing the fraction of clusters that does not undergo spin relaxation, and thus contribute to the symmetric beamlets, to be below the detection limit. Indeed, the larger a cluster becomes, the more vibrational modes it has and thus the lower the probability that the cluster is in the vibrational ground state. Atomic-like splitting into beamlets only takes place when spin relaxation is inhibited. Otherwise, spin relaxation results in single-sided deflection. On top of this there is a strong cluster dependence as particularly the presence of soft vibrational modes strongly reduces the population of the vibrational ground state. Also, in the doped species, a non-zero orbital magnetic moment of the localized cobalt  $3d$  orbitals [29] could additionally contribute to the spin relaxation via spin-orbit coupling. This can explain the relatively lower fraction of deflected cobalt doped clusters relative to pure silver clusters consisting of the same number of atoms.

In contrast to neutral  $\text{CoAg}_n$  clusters, all  $\text{CoAg}_n^+$  clusters with  $n = 2-9$  show a considerable magnetic response since a finite XMCD asymmetry is observed. Only for clusters with  $n = 10-12$  the XMCD signal vanishes. As mentioned above, the XMCD signal at the cobalt  $L_3$  edge results from the local magnetic moment at the cobalt site. It is moreover possible to obtain information on the global magnetic moment as the XMCD intensity is scaled by the magnetization of the cluster, which is a Brillouin function  $\mathcal{B}(\mu_{\text{cluster}}, T, B)$  of the cluster global magnetic moment as well as of cluster temperature  $T$  and the strength of the applied magnetic field  $B$  [27,30]. The observed XMCD signal for the smaller clusters therefore indicates both a nonzero global and local (cobalt  $3d$ ) magnetic moment. For the larger clusters, the missing XMCD signal indicates that  $\text{CoAg}_{10}^+$  and  $\text{CoAg}_{12}^+$  have a singlet ground state and  $\text{CoAg}_{11}^+$  has a low-spin  $S = 1/2$  ground state. Furthermore, the missing cobalt  $2p$  XMCD signal for  $\text{CoAg}_{11}^+$  demonstrates that the unpaired spin has essentially no localized cobalt  $3d$  character but is of  $s$  character and delocalized over the cluster, consistent with the single occupation of the  $2S$  cluster electron shell for a 19 electron system. From the measured relative XMCD amplitude and the lowest possible ion temperatures in the ion trap, we can discard low-spin states for  $\text{CoAg}_n^+$  clusters with  $n \leq 8$  and therefore propose  $S = 1$  and  $S = 3/2$  states for even and odd  $n$ , respectively. The high-spin ground state, together with strong multiplet splitting, indicates that the cobalt  $3d$  orbitals remain localized at the cobalt site, which is in line with the simulations for  $n \leq 6$  [cf. Fig. 2(b)]. For  $n = 7, 8$  the spectral shape of the x-ray absorption spectrum and the non-integer  $3d$  occupation indicate that slight hybridization with silver  $5s$  and/or  $4d$  orbitals occurs. For  $n = 9$  a high-spin ground state with  $S = 3/2$  is proposed, in line with the simulation, demonstrating that no or only little delocalization induced by  $\text{Co}(3d) - \text{Ag}(5s/4d)$  hybridization takes place. In this 17 valence electron system, seven electrons remain localized at the cobalt impurity in a  $3d^7$  configuration, while the remaining ten electrons are mostly of  $s$  character (cobalt  $4s$  and silver  $5s$ ) and delocalized over the whole cluster.

TABLE I. Most plausible spin state for neutral  $\text{CoAg}_n$  and cationic  $\text{CoAg}_n^+$  clusters as proposed from experiments and cobalt  $3d$  occupation of  $\text{CoAg}_n^+$ . Spin states given in brackets can not be excluded.

Cluster size $n$	Spin state $S$		Co $3d$ occupancy
	Neutral	Cationic	Cationic
2		1	8
3		3/2	7
4	1/2 (3/2)	1	8
5	1	3/2	7
6	1/2	1	8
7	1 (0)	3/2	7.3
8	1/2	1	7.3
9	0	3/2	7
10	1/2	0	8.6
11	0	1/2	8.6
12	1/2	0	8.6
13	0		
14	1/2		
15	0		

The proposed spin states for the neutral  $\text{CoAg}_n$  and cationic  $\text{CoAg}_n^+$  clusters are summarized in Table I.

A detailed analysis of the proposed unique electronic structure of  $\text{CoAg}_9^+$  is discussed in the following. In Fig. 3 the calculated density of states (DOS) for the proposed 10 (delocalized) + 7 (localized) electron system  $\text{CoAg}_9^+$  is shown and for comparison also the DOS of  $\text{CoAg}_{10}^+$  and of the endohedral isomer of neutral  $\text{CoAg}_9$ , which both are 18 delocalized electron systems. For both cationic  $\text{CoAg}_{10}^+$  and neutral  $\text{CoAg}_9$ , the delocalization of all 18 valence electrons leads to a closed electronic shell configuration with  $S = 0$  and the grouping of electrons into shells can be inferred from the DOS, in line with previous predictions based on mass spectrometric data [14]. Detailed examination of the DOS and corresponding orbitals of the isoelectronic  $\text{CoAg}_9$  and  $\text{CoAg}_{10}^+$  clusters allow identifying the expected  $1S^2, 1P^6, 1D^{10}, 2S^2 \dots$  orbitals, with a large HOMO-LUMO gap between  $1D$  and  $2S$  for these closed 18 electron shell clusters. (We use italic capital letters to refer to cluster shell model electron orbitals.) This also implies that the magnetic moment of the endohedral cobalt atom will be quenched, and hence also the total magnetic moment (see below).

In the case of cationic  $\text{CoAg}_9^+$ , the calculation suggests that  $1S, 1P$ , and  $1D$  electronic shells are formed. The  $1P$  level, containing six electrons that mainly originate from silver  $5s$  electrons, is fully occupied but the level degeneracy is lifted because of the low symmetry of the cluster. Two delocalized electrons occupy the  $1D_{xy}$  (sub)shell, which has mixed silver-cobalt character. In total the electron cloud consists of ten delocalized electrons, while seven cobalt  $3d$  electrons remain localized. The localized molecular orbitals are depicted at the bottom of Fig. 3. This assignment is in agreement with the local  $3d^7$  configuration inferred above from the comparison of the measured and simulated x-ray absorption spectra at the cobalt  $L_3$  edge.

### C. Interplay of geometry, impurity–host-state hybridization and electron count on spin states of cobalt doped silver clusters

In our x-ray absorption spectroscopy study of  $\text{CoAg}_n^+$  clusters with  $n = 2-12$ , we observe a strong change of the spectral shape and a vanishing XMCD signal for  $\text{CoAg}_n^+$  clusters with  $n \geq 10$  as can be seen in Fig. 2, where the cobalt impurity is encapsulated by the silver atoms, and the doping becomes endohedral as is known for cationic species from photofragmentation [14] and reactivity [18,19] studies and predicted for neutral species by computational [22,24] studies. A clear correlation of the shape of the x-ray absorption spectrum, shift of excitation energy, and vanishing local magnetic moment with the onset of dopant encapsulation has been previously observed in manganese-doped silicon clusters [10]. However, in contrast to  $\text{CoAg}_n^+$  where the dopant electrons contribute to delocalized states of the free electron gas, the molecular orbitals in  $\text{MnSi}_n^+$  are not well described by a free electron gas due to the covalent bonding in the silicon host. We also identify a size regime in cationic  $\text{CoAg}_n^+$  clusters ( $n = 7, 9$ ) of intermediate  $3d-5s$  hybridization strength similar to what has been predicted for  $\text{VAg}_n$  clusters [16]. This size range coincides with the predicted cluster-size dependent transition from two to three dimensional structures in other (neutral) transition metal doped silver clusters [16,17,22,23]. According to the predictions, this structural transition is accompanied by the onset of a partial encapsulation of the dopant atom.  $\text{CoAg}_9^+$  stands out by a low  $3d-5s$  hybridization, which goes along with its exohedral ground-state geometry.

Regarding the electronic structure, the exohedral size regime is characterized by a weak perturbation of the cobalt  $3d$  orbitals from the atomic limit as x-ray absorption spectra can be simulated by symmetry adapted atomic Hartree-Fock calculations. Hence, there is no pronounced hybridization, such that the cobalt  $3d$  orbitals remain largely nonbonding, localized at the cobalt site and forming a high-spin ground state. The alternating spectral shape and excitation energy of the cobalt  $L_3$  resonance (see Fig. S5 within the Supplemental Material [46]) reflects an alternating nominal  $3d$  occupation as extracted from comparison to our simulations.

Our results show that the cobalt  $3d$  occupation adapts to the number of silver valence electrons, as to always give an even number of delocalized valence electrons in the cluster, but does not depend considerably on the atomic environment of the dopant. This ultimately defines the spin magnetic moment of the exohedral clusters. A similar odd-even pattern of the  $L_3$  onset (that is related to the  $3d$  occupation [54]) and alternating  $3d$  configuration has been observed previously for exohedrally titanium-doped gold clusters [9]. The atomic environment of the dopant is predicted to vary strongly as the number of silver atoms increases. It is worth mentioning that for small exohedral clusters  $\text{CoAg}_n^{0,+}$   $n = 2-6$  spin polarization of the silver host is incompatible with the local  $3d$  electron population and the spin ground states as deduced from the XAS and XMCD measurements. Negligible spin polarization of the host is also compatible with the inhibited spin relaxation, which leads to the atomic-like Stern-Gerlach deflection observed for  $n = 6$  and 8. All this is in contrast to DFT studies on  $\text{CoAg}_n$  clusters reporting sizable spin polarization at the host [24], which might be due to the known tendency of DFT to overestimate delocalization of  $3d$  orbitals,

see Ref. [55] and references therein. The electronic structure in the endohedral regime is characterized by a strong intra-cluster  $3d-5s$  interaction between the cobalt impurity and the silver host as evidenced by the emergence of a satellite line in x-ray absorption spectroscopy [56,57]. Consequently, our charge transfer multiplet calculations involve large hopping terms. In line with the strong hybridization, the median of the excitation energy shifts to higher energy by  $\approx 0.5$  eV, see Fig. S5 within the Supplemental Material [46]. In contrast to endohedrally doped silicon clusters where significant covalent bonding of the host atoms leads to a strong size dependence of the dopant electronic structure [10], here we find very little size dependence of the dopant's local electronic structure. This can be understood by the formation of hybridized cluster orbitals instead of directional bonds as in manganese-doped silicon clusters, leading to strong delocalization of the cobalt  $3d$  electron density and to a low-spin ground state.

With respect to spin multiplicity, the encapsulation of the cobalt impurity by the silver host has a similar effect on the magnetic moment for both neutral and charged clusters. Hybridization leads to a quenching of the impurity magnetic moment and therefore to a low-spin ground state as observed for cobalt impurities in bulk silver [58]. The remaining single spin in the larger odd-electron clusters with a doublet ground state is likely delocalized and spin relaxation is effective as evidenced by the absence of symmetric deflection beamlets. Interestingly, while in  $\text{CoAg}_{9-12}^+$  clusters the arrangement of some or all electrons into electronic shells contributes to stabilization, the effect on the magnetic moment is very different for exohedral  $\text{CoAg}_9^+$  and endohedral  $\text{CoAg}_{10-12}^+$ . In exohedral  $\text{CoAg}_9^+$  spin pairing of delocalized valence electrons involves only ten electrons and the remaining seven valence electrons do not participate but remain instead localized at the cobalt impurity, leading to a high-spin  $S = 3/2$  state. In the endohedral  $\text{CoAg}_{10-12}^+$  on the other hand, all valence electrons delocalize, participating in the filling of the electronic shells leading to low-spin states. The high to low spin transition observed from exohedral to endohedral clusters is consistent with the strong blue shift observed in the x-ray absorption (see Fig. S5 within the Supplemental Material [46]) [59,60].

In Fig. 4 the proposed spin states for cationic and neutral  $\text{CoAg}_n$  clusters are plotted against the nominal number of valence electrons (Ag  $5s$ , Co  $3d$  and  $4s$ ) that is a better descriptor than the number of silver atoms. For larger clusters with more than 17 valence electrons, the spin state is the lowest possible, with an odd-even alternation for neutral and cationic species. In contrast, for smaller clusters the spin state is intermediate for neutral species and high for cationic species. The magnetic impurity acts as a reservoir of electrons for the complete filling of the low-energy states of the free electron gas [8,9]. In the cationic species with 13 valence electrons,  $\text{CoAg}_5^+$ , only seven electrons remain localized in  $3d$  orbitals thus achieving spin pairing in the free electron gas consisting of six delocalized electrons (silver  $5s$  hybridized with cobalt  $4s$ ). The local cobalt  $3d^7$  configuration leads to a quartet spin state as observed via x-ray spectroscopy. As mentioned above,  $\text{CoAg}_9^+$  with 17 valence electrons is a special case as the spin pairing achieved by 10 delocalized electrons of cobalt  $4s$  and silver  $5s$  character without involvement of the seven  $3d$  electrons

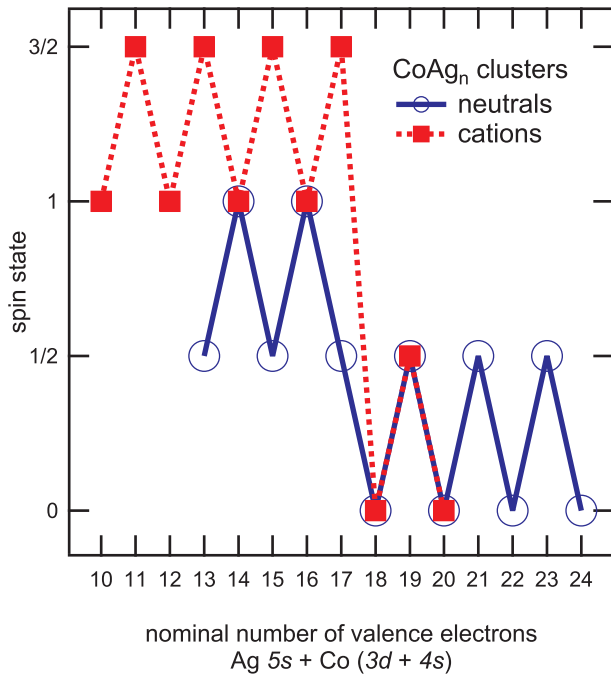


FIG. 4. Spin state  $S$  of  $\text{CoAg}_n^{0,+}$  clusters as suggested from Stern-Gerlach and x-ray spectroscopy studies as a function of the nominal number of valence electrons. While high spin states are found for cationic  $\text{CoAg}_n^+$  clusters with a nominal number of valence electrons  $\leq 17$ , only intermediate spin states are found for neutral  $\text{CoAg}_n$  with the same nominal number of valence electrons. For a number of valence electrons  $\geq 18$  both neutral and cationic clusters adopt the lowest possible spin state for the given number of electrons.

additionally stabilizes the quartet state from the local  $3d^7$  configuration. The neutral clusters with 13 and 15 valence electrons,  $\text{CoAg}_4$  and  $\text{CoAg}_6$ , require no delocalization of  $3d$  electrons from the magnetic impurity to attain four and six delocalized  $s$  valence electrons, respectively. Hence, cobalt assumes a  $3d^9$  configuration, leaving only one unpaired spin in agreement with the observed deflection of a doublet spin state. In summary, for exohedral clusters with odd number of valence electrons, the impurity acts as electron donor to the delocalized electron gas in cations but as an acceptor of redundant electrons in neutrals resulting in lower spin states for the latter.

## VI. CONCLUSIONS

We have investigated the size-dependent magnetic properties and electronic structure of neutral and cationic cobalt-doped silver clusters,  $\text{CoAg}_n^{0,+}$ , in the few-atom size range. We found that clusters with more than nine silver atoms

are low-spin systems independent of their charge state, coincident with the increase in stability and decrease in reactivity of endohedrally doped silver clusters. The encapsulation of the cobalt impurity by the nonmagnetic host with delocalized electrons goes along with strong hybridization of silver  $5s$  and cobalt  $4s/3d$  orbitals driven by the tendency to form a free electron gas, resulting in delocalized electronic states that lead to quenched local  $3d$  magnetic moments and low-spin ground states. Moreover, endohedrally doped clusters with a doublet state show enhanced spin relaxation when compared to pure silver clusters. In exohedral clusters the spin magnetic moment of the cluster is determined by spin pairing of valence electrons of the host that results in high and intermediate spin states in cationic and neutral clusters, respectively.

A combined experimental study of cationic and neutral clusters was reported, providing evidence about the evolution with cluster size of the magnetic moment of noble metal clusters with a single magnetic dopant. This study shows that quenching of magnetism in small cobalt-doped silver clusters that are fully encapsulated is due to strong hybridization of cobalt  $4s/3d$  orbitals with the silver  $5s$  valence electrons, leading to an electronic shell closure for  $\text{CoAg}_{10}^+$  and corresponding to a high density of states at the Fermi level, which is consistent with the underlying physics predicted for early transition-metal doped coinage metal clusters. These observations provide fundamental insight in the interaction of magnetic atoms with nonmagnetic hosts, in the limit of very small nano-objects.

## ACKNOWLEDGMENTS

This work is supported by the KU Leuven Research Council (Projects No. C14/18/073 and No. C14/22/103). P.F. thanks the FWO for a postdoctoral grant. Beamtime for this project was granted at BESSY II beamline UE52-PGM, operated by Helmholtz-Zentrum Berlin. The superconducting magnet was provided by Toyota Technological Institute. A.T. acknowledges financial support by Genesis Research Institute, Inc. The Ion Trap end station at UE52-PGM was partially supported by BMBF Grant No. 05K16VF1.

B.v.I., P.L., W.A.d.H., J.T.L., E.J., K.H., and V.Z.B. conceptualized the work. V.Z.B., L.M., K.D.K., and X.X. analyzed the data. K.H. and P.F. performed the simulations. V.Z.B., L.M., K.H., X.X., A.L., and J.T.L. performed the experiments and validated the data. V.Z.B. wrote the original draft of the manuscript that was reviewed and edited by V.Z.B., K.H., K.D.K., A.T., P.F., B.v.I., P.L., J.T.L., and E.J. B.v.I., P.L., W.A.d.H., J.T.L., and E.J. acquired funding for the project. B.v.I., P.L., W.A.d.H., J.T.L., and E.J. coordinated and supervised the project.

- [1] D. Goldhaber-Gordon, H. Shtrikman, D. Mahalu, D. Abusch-Magder, U. Meirav, and M. A. Kastner, Kondo effect in a single-electron transistor, *Nature (London)* **391**, 156 (1998).
- [2] E. Coronado, Molecular magnetism: from chemical design to spin control in molecules, materials and devices, *Nat. Rev. Mater.* **5**, 87 (2020).

- [3] G. Gruner and A. Zawadowski, Magnetic impurities in non-magnetic metals, *Rep. Prog. Phys.* **37**, 1497 (1974).
- [4] J. Kondo, Resistance minimum in dilute magnetic alloys, *Prog. Theor. Phys.* **32**, 37 (1964).
- [5] P. W. Anderson, Localized magnetic states in metals, *Phys. Rev.* **124**, 41 (1961).



- [6] M. Ternes, A. J. Heinrich, and W.-D. Schneider, Spectroscopic manifestations of the Kondo effect on single adatoms, *J. Phys.: Condens. Matter* **21**, 053001 (2009).
- [7] J. Nygård, D. H. Cobden, and P. E. Lindelof, Kondo physics in carbon nanotubes, *Nature (London)* **408**, 342 (2000).
- [8] K. Hirsch, V. Zamudio-Bayer, A. Langenberg, M. Niemeyer, B. Langbehn, T. Möller, A. Terasaki, B. v. Issendorff, and J. T. Lau, Magnetic Moments of Chromium-Doped Gold Clusters: The Anderson Impurity Model in Finite Systems, *Phys. Rev. Lett.* **114**, 087202 (2015).
- [9] K. Hirsch, V. Zamudio-Bayer, A. Langenberg, M. Vogel, J. Rittmann, S. Forin, T. Möller, B. v. Issendorff, and J. T. Lau, Impurity electron localization in early-transition-metal-doped gold clusters, *J. Phys. Chem. C* **119**, 11184 (2015).
- [10] V. Zamudio-Bayer, L. Leppert, K. Hirsch, A. Langenberg, J. Rittmann, M. Kossick, M. Vogel, R. Richter, A. Terasaki, T. Möller, B. v. Issendorff, S. Kümmel, and J. T. Lau, Coordination-driven magnetic-to-nonmagnetic transition in manganese-doped silicon clusters, *Phys. Rev. B* **88**, 115425 (2013).
- [11] A. Diaz-Bachs, L. Peters, R. Logemann, V. Chernyy, J. M. Bakker, M. I. Katsnelson, and A. Kirilyuk, Magnetic properties of Co-doped Nb clusters, *Phys. Rev. B* **97**, 134427 (2018).
- [12] U. Rohrmann and R. Schäfer, Stern-Gerlach Experiments on Mn@Sn<sub>12</sub>: Identification of a Paramagnetic Superatom and Vibrationally Induced Spin Orientation, *Phys. Rev. Lett.* **111**, 133401 (2013).
- [13] K. J. Taylor, C. L. Pettiette-Hall, O. Cheshnovsky, and R. E. Smalley, Ultraviolet photoelectron spectra of coinage metal clusters, *J. Chem. Phys.* **96**, 3319 (1992).
- [14] E. Janssens, S. Neukermans, H. M. T. Nguyen, M. T. Nguyen, and P. Lievens, Quenching of the Magnetic Moment of a Transition Metal Dopant in Silver Clusters, *Phys. Rev. Lett.* **94**, 113401 (2005).
- [15] K. Tono, A. Terasaki, T. Ohta, and T. Kondow, Photoelectron spectroscopy and density-functional calculations of silver cluster anions doped with a cobalt atom: Size dependent sp-d interaction, *Chem. Phys. Lett.* **449**, 276 (2007).
- [16] V. M. Medel, A. C. Reber, V. Chauhan, P. Sen, A. M. Köster, P. Calaminici, and S. N. Khanna, Nature of valence transition and spin moment in Ag<sub>n</sub>V<sup>+</sup> clusters, *J. Am. Chem. Soc.* **136**, 8229 (2014).
- [17] W. H. Blades, A. C. Reber, S. N. Khanna, L. López-Sosa, P. Calaminici, and A. M. Köster, Evolution of the spin magnetic moments and atomic valence of Vanadium in VCu<sub>x</sub><sup>+</sup>, VAg<sub>x</sub><sup>+</sup>, and VAu<sub>x</sub><sup>+</sup> clusters ( $x = 3-14$ ), *J. Phys. Chem. A* **121**, 2990 (2017).
- [18] S. Sarugaku, M. Arakawa, T. Kawano, and A. Terasaki, Electronic and geometric effects on chemical reactivity of 3d-transition-metal-doped silver cluster cations toward oxygen molecules, *J. Phys. Chem. C* **123**, 25890 (2019).
- [19] K. Minamikawa, M. Arakawa, K. Tono, and A. Terasaki, A revisit to electronic structures of cobalt-doped silver cluster anions by size-dependent reactivity measurement, *Chem. Phys. Lett.* **753**, 137613 (2020).
- [20] M. Arakawa, M. Horioka, K. Minamikawa, T. Kawano, and A. Terasaki, Reaction of nitric oxide molecules on transition-metal-doped silver cluster cations: Size- and dopant-dependent reaction pathways, *Phys. Chem. Chem. Phys.* **23**, 22947 (2021).
- [21] K. Minamikawa, S. Sarugaku, M. Arakawa, and A. Terasaki, Electron counting in cationic and anionic silver clusters doped with a 3d transition-metal atom: Endo- vs. exohedral geometry, *Phys. Chem. Chem. Phys.* **24**, 1447 (2022).
- [22] P. Marín, J. A. Alonso, E. Germán, and M. J. López, Nanoalloys of metals which do not form bulk alloys: The case of Ag-Co, *J. Phys. Chem. A* **124**, 6468 (2020).
- [23] N. T. Mai, N. T. Lan, N. T. Cuong, N. M. Tam, S. T. Ngo, T. T. Phung, N. V. Dang, and N. T. Tung, Systematic investigation of the structure, stability, and spin magnetic moment of CrM<sub>n</sub> clusters (M = Cu, Ag, Au, and  $n = 2-20$ ) by DFT calculations, *ACS Omega* **6**, 20341 (2021).
- [24] P. Rodríguez-Kessler and A. Rodríguez-Domínguez, Structural, electronic, and magnetic properties of Ag<sub>n</sub>Co ( $n=1-9$ ) clusters: A first-principles study, *Comput. Theor. Chem.* **1066**, 55 (2015).
- [25] K. Clemenger, Ellipsoidal shell structure in free-electron metal clusters, *Phys. Rev. B* **32**, 1359 (1985).
- [26] J. Zhao, X. Huang, P. Jin, and Z. Chen, Magnetic properties of atomic clusters and endohedral metallofullerenes, *Coord. Chem. Rev.* **289-290**, 315 (2015).
- [27] A. Langenberg, K. Hirsch, A. Ławicki, V. Zamudio-Bayer, M. Niemeyer, P. Chmiela, B. Langbehn, A. Terasaki, B. v. Issendorff, and J. T. Lau, Spin and orbital magnetic moments of size-selected iron, cobalt, and nickel clusters, *Phys. Rev. B* **90**, 184420 (2014).
- [28] J. Meyer, M. Tombers, C. van Wüllen, G. Niedner-Schatteburg, S. Peredkov, W. Eberhardt, M. Neeb, S. Palutke, M. Martins, and W. Wurth, The spin and orbital contributions to the total magnetic moments of free Fe, Co, and Ni clusters, *J. Chem. Phys.* **143**, 104302 (2015).
- [29] V. Zamudio-Bayer, K. Hirsch, A. Langenberg, A. Ławicki, A. Terasaki, B. von Issendorff, and J. T. Lau, Large orbital magnetic moments of small, free cobalt cluster ions Co<sub>n</sub><sup>+</sup> with  $n \leq 9$ , *J. Phys.: Condens. Matter* **30**, 464002 (2018).
- [30] M. Niemeyer, K. Hirsch, V. Zamudio-Bayer, A. Langenberg, M. Vogel, M. Kossick, C. Ebrecht, K. Egashira, A. Terasaki, T. Möller, B. v. Issendorff, and J. T. Lau, Spin Coupling and Orbital Angular Momentum Quenching in Free Iron Clusters, *Phys. Rev. Lett.* **108**, 057201 (2012).
- [31] A. Diaz-Bachs, M. I. Katsnelson, and A. Kirilyuk, Kramers degeneracy and relaxation in vanadium, niobium and tantalum clusters, *New J. Phys.* **20**, 043042 (2018).
- [32] U. Rohrmann, P. Schwerdtfeger, and R. Schäfer, Atomic domain magnetic nanoalloys: Interplay between molecular structure and temperature dependent magnetic and dielectric properties in manganese doped tin clusters, *Phys. Chem. Phys.* **16**, 23952 (2014).
- [33] T. M. Fuchs and R. Schäfer, Double Stern-Gerlach experiments on Mn@Sn<sub>12</sub>: Refocusing of a paramagnetic superatom, *Phys. Rev. A* **98**, 063411 (2018).
- [34] M. Gleditsch, T. M. Fuchs, and R. Schäfer, N-doping at the sub-nanoscale: Dielectric and magnetic response of neutral phosphorus-doped tin clusters, *J. Phys. Chem. A* **123**, 1434 (2019).
- [35] R. Moro, X. Xu, S. Yin, and W. A. de Heer, Ferroelectricity in free niobium clusters, *Science* **300**, 1265 (2003).
- [36] X. Xu, S. Yin, R. Moro, and W. A. de Heer, Magnetic Moments and Adiabatic Magnetization of Free Cobalt Clusters, *Phys. Rev. Lett.* **95**, 237209 (2005).
- [37] W. A. de Heer and P. Milani, Large ion volume time-of-flight mass spectrometer with position- and velocity-sensitive

- detection capabilities for cluster beams, *Rev. Sci. Instrum.* **62**, 670 (1991).
- [38] K. Hirsch, J. T. Lau, P. Klar, A. Langenberg, J. Probst, J. Rittmann, M. Vogel, V. Zamudio-Bayer, T. Möller, and B. v. Issendorff, X-ray spectroscopy on size-selected clusters in an ion trap: from the molecular limit to bulk properties, *J. Phys. B: At. Mol. Opt. Phys.* **42**, 154029 (2009).
- [39] F. Neese, The ORCA program system, *WIREs Comput. Mol. Sci.* **2**, 73 (2012).
- [40] J. P. Perdew, K. Burke, and M. Ernzerhof, Generalized Gradient Approximation Made Simple, *Phys. Rev. Lett.* **77**, 3865 (1996).
- [41] F. Weigend and R. Ahlrichs, Balanced basis sets of split valence, triple zeta valence and quadruple zeta valence quality for H to Rn: Design and assessment of accuracy, *Phys. Chem. Chem. Phys.* **7**, 3297 (2005).
- [42] D. Andrae, U. Häußermann, M. Dolg, H. Stoll, and H. Preuß, Energy-adjusted *ab initio* pseudopotentials for the second and third row transition elements, *Theor. Chim. Acta* **77**, 123 (1990).
- [43] S. Grimme, J. Antony, S. Ehrlich, and H. Krieg, A consistent and accurate *ab initio* parametrization of density functional dispersion correction (DFT-D) for the 94 elements H-Pu, *J. Chem. Phys.* **132**, 154104 (2010).
- [44] S. Grimme, S. Ehrlich, and L. Goerigk, Effect of the damping function in dispersion corrected density functional theory, *J. Comput. Chem.* **32**, 1456 (2011).
- [45] E. Stavitski and F. M. de Groot, The CTM4XAS program for EELS and XAS spectral shape analysis of transition metal L edges, *Micron* **41**, 687 (2010).
- [46] See Supplemental Material at <http://link.aps.org/supplemental/10.1103/PhysRevResearch.5.033103> for Stern-Gerlach profiles of pure silver clusters, parameters of the CTM4XAS calculations, detailed analysis of deflection profiles, and analysis of  $L_3$  edge resonance energy as a function of cluster size.
- [47] R. Dong, X. Chen, H. Zhao, X. Wang, H. Shu, Z. Ding, and L. Wei, Structural, electronic and magnetic properties of  $Ag_nFe$  clusters ( $n \leq 15$ ): Local magnetic moment interacting with delocalized electrons, *J. Phys. B: At. Mol. Opt. Phys.* **44**, 035102 (2011).
- [48] G. van der Laan, B. T. Thole, G. A. Sawatzky, and M. Verdaguer, Multiplet structure in the  $L_{2,3}$  x-ray-absorption spectra: A fingerprint for high- and low-spin  $Ni^{2+}$  compounds, *Phys. Rev. B* **37**, 6587 (1988).
- [49] G. van der Laan and I. W. Kirkman, The  $2p$  absorption spectra of  $3d$  transition metal compounds in tetrahedral and octahedral symmetry, *J. Phys.: Condens. Matter* **4**, 4189 (1992).
- [50] E. M. Fernández, J. M. Soler, I. L. Garzón, and L. C. Balbás, Trends in the structure and bonding of noble metal clusters, *Phys. Rev. B* **70**, 165403 (2004).
- [51] J. van der Tol, D. Jia, Y. Li, V. Chernyy, J. M. Bakker, M. T. Nguyen, P. Lievens, and E. Janssens, Structural assignment of small cationic silver clusters by far-infrared spectroscopy and DFT calculations, *Phys. Chem. Chem. Phys.* **19**, 19360 (2017).
- [52] X.-J. Hou, E. Janssens, P. Lievens, and M. T. Nguyen, Theoretical study of the geometric and electronic structure of neutral and anionic doped silver clusters,  $Ag_5X^{0,-}$  with  $X = Sc, Ti, V, Cr, Mn, Fe, Co,$  and  $Ni$ , *Chem. Phys.* **330**, 365 (2006).
- [53] W. A. de Heer, The physics of simple metal clusters: experimental aspects and simple models, *Rev. Mod. Phys.* **65**, 611 (1993).
- [54] M. Flach, K. Hirsch, M. Timm, O. S. Ablyasova, M. da Silva Santos, M. Kubin, C. Bülow, T. Gitzinger, B. von Issendorff, J. T. Lau, and V. Zamudio-Bayer, Iron  $L_3$ -edge energy shifts for the full range of possible  $3d$  occupations within the same oxidation state of iron halides, *Phys. Chem. Chem. Phys.* **24**, 19890 (2022).
- [55] P. Mori-Sánchez, A. J. Cohen, and W. Yang, Many-electron self-interaction error in approximate density functionals, *J. Chem. Phys.* **125**, 201102 (2006).
- [56] M.-A. Arrio, P. Saintavit, C. Cartier dit Moulin, T. Mallah, M. Verdaguer, E. Pellegrin, and C. T. Chen, Characterization of chemical bonds in bimetallic cyanides using x-ray absorption spectroscopy at  $L_{2,3}$  edges, *J. Am. Chem. Soc.* **118**, 6422 (1996).
- [57] T. Hatsui, Y. Takata, N. Kosugi, K. Yamamoto, T. Yokoyama, and T. Ohta, Ni  $2p$  excitation spectra of some planar Ni complexes, *J. Electron Spectrosc. Relat. Phenom.* **88–91**, 405 (1998).
- [58] D. Riegel and K. Gross, Magnetism and electronic structure of  $3d$  and  $4d$  ions in metals, *Phys. B: Condens. Matter* **163**, 678 (1990).
- [59] T. L. Daulton and B. J. Little, Determination of chromium valence over the range Cr(0)-Cr(VI) by electron energy loss spectroscopy, *Ultramicroscopy* **106**, 561 (2006).
- [60] S. T. Akin, V. Zamudio-Bayer, K. Duanmu, G. Leistner, K. Hirsch, C. Bülow, A. Ławicki, A. Terasaki, B. von Issendorff, D. G. Truhlar *et al.*, Size-dependent ligand quenching of ferromagnetism in  $Co_3(\text{benzene})_n^+$  clusters studied with x-ray magnetic circular dichroism spectroscopy, *J. Phys. Chem. Lett.* **7**, 4568 (2016).